Observations of rotational motions in the P coda of seismic signals

D.N. Pham[1,2], H. Igel[1]

(1) Geophysics Section, Department of Earth and Environmental Sciences, LMU Muenchen, GERMANY
(2) Institute of Geophysics, VAST, Hanoi, VIETNAM

The collocated observations of rotations around a vertical axis and translations obtained by a 4x4m ring laser and traditional broad band seismometer recently in Germany provided a database of 20 events, each includes 3 classical components of ground velocity and a vertical component of ground rotation. The epicentral distance and magnitude distributions of these observed events are shown in figure 1.

Analysis of the observed data showed that in some big events the vertical rotation signals are visible in the P coda sections (table 1, see also Igel et al., 2007). A typical example for this observation is the case of the Sumatra earthquake 26/12/2004, M9.3 given in figure 2. Using low-pass filter and gradually increasing the cut-off period we can see the amplitude of the P coda rotations is also gradually decreased. The P coda rotational signals almost disappear when the cut-off period reaches a value of 10 s. This implies that energy of P coda rotations is predominant in the high frequency range.

However in some other smaller events (table 1), such as the Gibraltar event 24/2/2004, M6.4 (figure 3, third trace from top), the phenomenon of P coda rotations is not visible due to the low signal to noise ratio. To investigate rotation rate in such events, we use the cross correlation technique. Theoretically, assuming plane wave propagation in horizontal direction with transverse polarization, rotation rate and transverse acceleration should have the same waveform and their amplitudes should scale proportionally to two times the phase velocity (Cochard et al., 2005; Igel et al., 2005, 2007). The zero lag normalized cross correlation coefficient - defined between 0 (no similarity) and 1 (perfect match) - between rotation rate and transversal acceleration was calculated for a sliding time window of appropriate length (at least twice the dominant period) along the time series. After high-pass filtering both signals (transversal acceleration and rotation rate), the calculated result revealed a clear increase of the coefficients coinciding with the onset of P waves (figure 3, bottom). The increase of the correlation coefficients between high-pass filtered rotation rate and transversal acceleration at the onset of P waves appears for all observed events (figure 4). We interpret this as the presence of SH type motions in the P coda.

In order to quantify and document this effect more clearly we calculate the zero-lag-normalized-cross-correlation-coefficients as a function of the cutoff period of the high pass filter applied before. Slide window lengths were taken twice as long as the cutoff periods. The cutoff period range was chosen from 0.5(s) to 10 (s) to cover the period bands of the directly arriving P – energy (around 1 s.) and S - energy (around 5 s.). The typical results are shown in the bottom of figures 5-10. In these figures, we can see a sharp increase in correlation at and following the direct P – wave. This correlation smears out and becomes less pronounced with increasing period, while the corresponding correlation of SH – type signals and Love waves increases with period.

All the above observations indicate that there are significant high frequency rotational motions in the P coda of seismic signals. Theoretically, in spherically symmetric isotropic media P and SV waves do not generate a vertical component of rotation so we should not observe this kind of motions before the arrival time of SH waves. The sensible explanation for these observed P coda rotations is 3D effects (P – SH scattering). So the questions to be addressed are:

- Can we generate synthetic seismograms (translation + rotation) that reproduce the observations?
- What kind of random media (correlation length, perturbation, etc) do we need to model the data?
- Where do we have to put scatterers?
- Do the observations of rotations (i.e. SH type motions) allow to constrain scattering properties?
- Are there tools (in addition to complete wave field modelling that is expensive in 3D) from scattering theory that allow the calculation of synthetic seismograms (include rotations)?

References

Cochard, A., Igel, H., Schuberth, B., Suryanto, W., Velikoseltsev, A., Schreiber, U., Wassermann, J., Scherbaum, F., Vollmer, D., 2005. Rotational motions in seismology: theory, observations, simulation, in *“Earthquake source asymmetry, structure media and rotation effects”* eds. Teisseyre et al., Springer Verlag.

Igel, H., Schreiber, U., Flaws, A., Schuberth, B., Velikoseltsev, J., Corchard, A., 2005. Rotational motions induced by the M8.1 Tokachi-oki earthquake, September 25, 2003, *Geophys. Res. Lett.*, **32**, L08309, doi: 10.1029/2004GL0223306.

Igel, H., Cochard, A., Wassermann, J., Flaws, A., Schreiber, U., Velikoseltsev, A., Pham, D.N., 2007. Broadband Observations of Earthquake Induced Rotational Ground Motions, *Geophys. J. Int.*, **168**, 182-196.

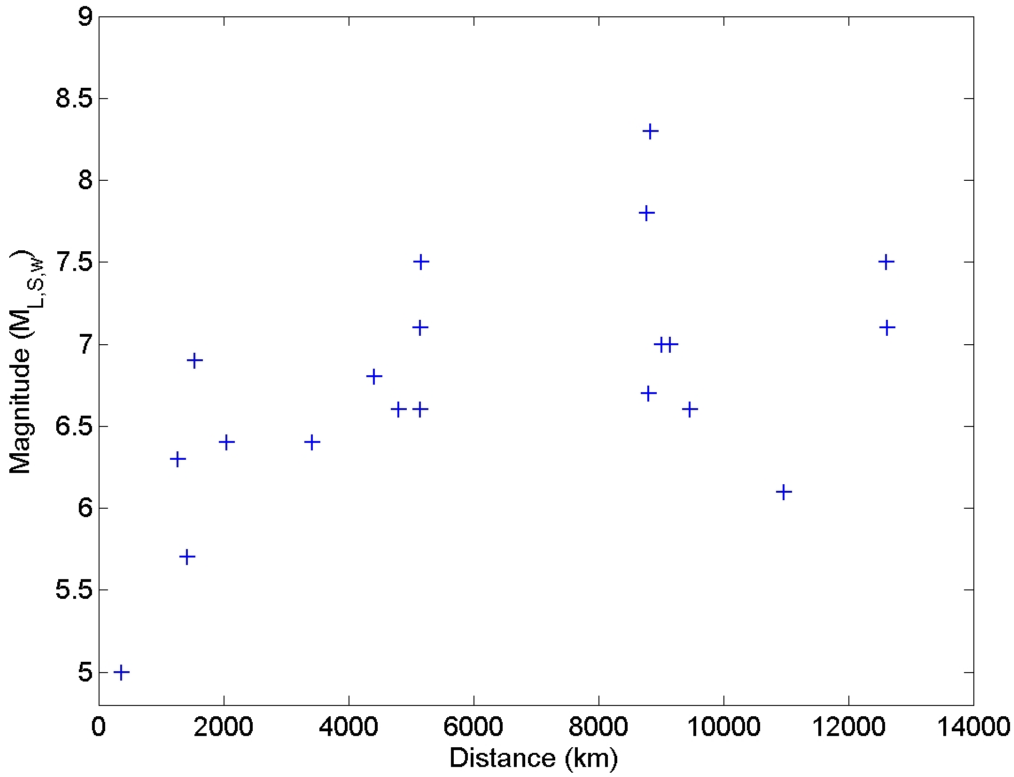

Figure 1. Magnitude distribution of processed events as a function of epicentral distance

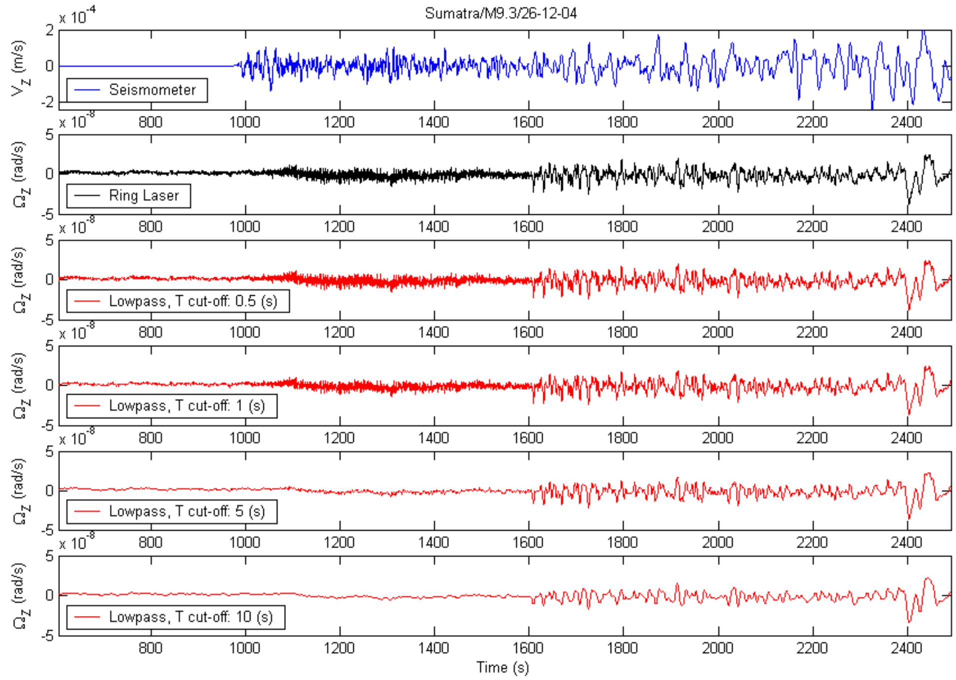

Figure 2. Observations of translational and rotational ground motions induced by Sumatra earthquake 26/12/2004, M9.3. Two top traces: Vertical component of ground velocity recorded by broadband seismometer and rotation rate in a vertical axis recorded by ring laser sensor. Four bottom traces: low-pass filtered rotation rate with different cut-off periods 0.5 s, 1 s, 5 s, 10 s. Significant energy in rotational motions in the P coda is visible. The connection between the decrease of the rotation amplitude and the increase of the cut-off period implies that the P coda rotations are predominantly in the high frequency range.

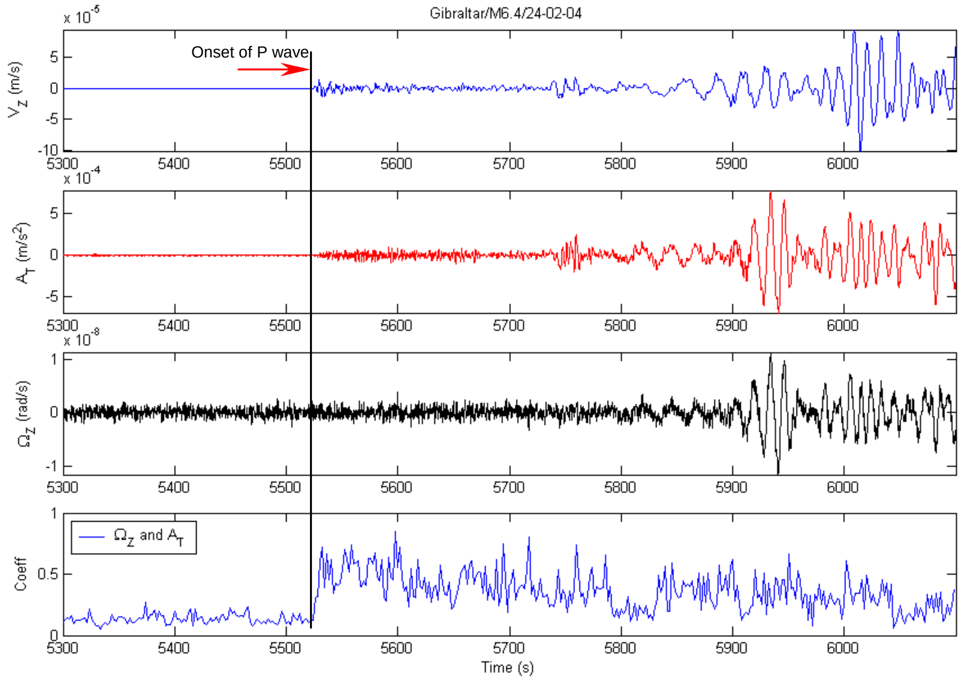

Figure 3. Gibraltar event 24/2/2004, M6.4. Top three traces: Vertical velocity, transverse acceleration and rotation rate, respectively. The bottom trace: zero lag normalized cross correlation coefficients between rotation rate and transverse acceleration after high-pass filtering with cut-off period 1s, calculated for time windows of 2s sliding along time series.

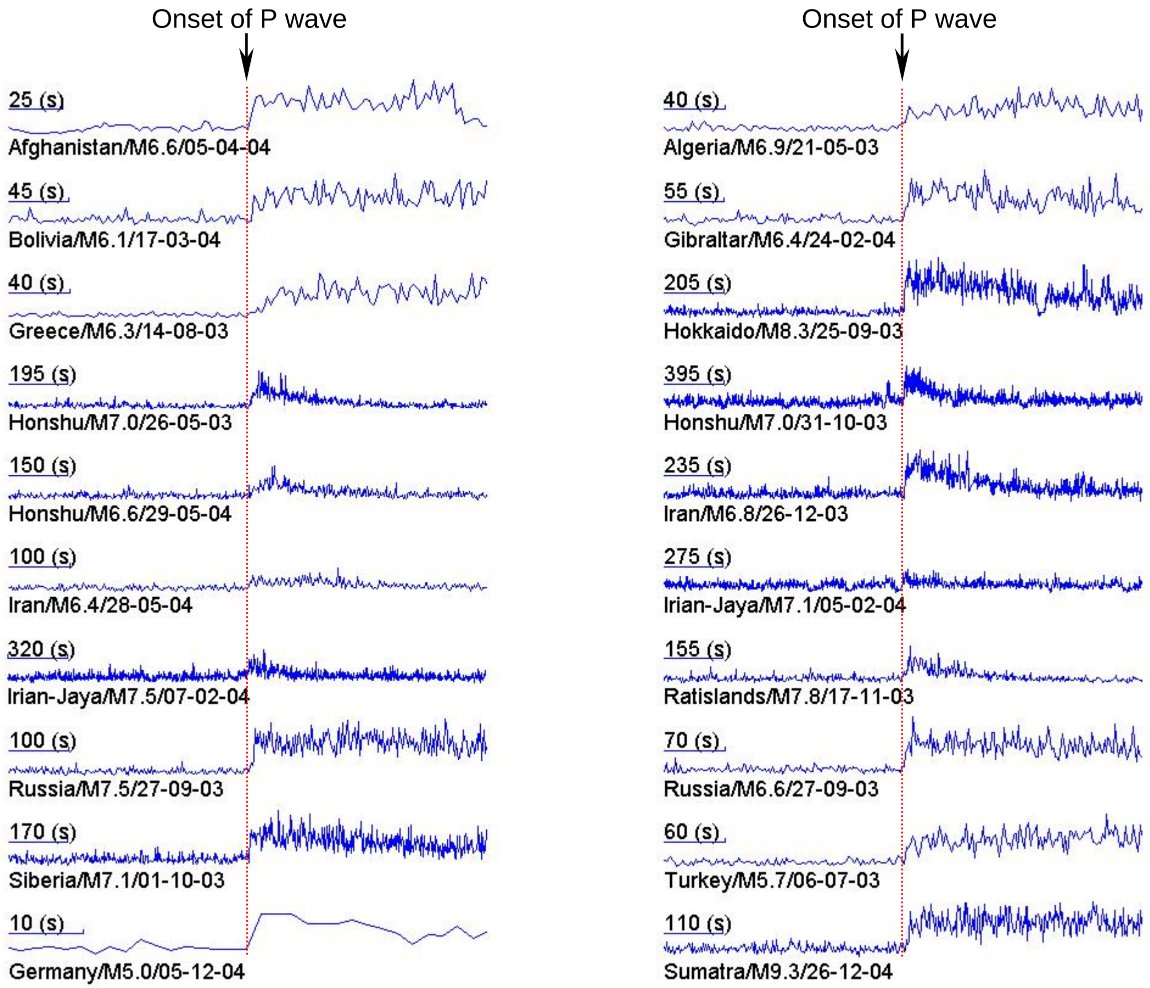

Figure 4. The normalized cross correlation coefficients increase at the onset of P waves in all observed events.

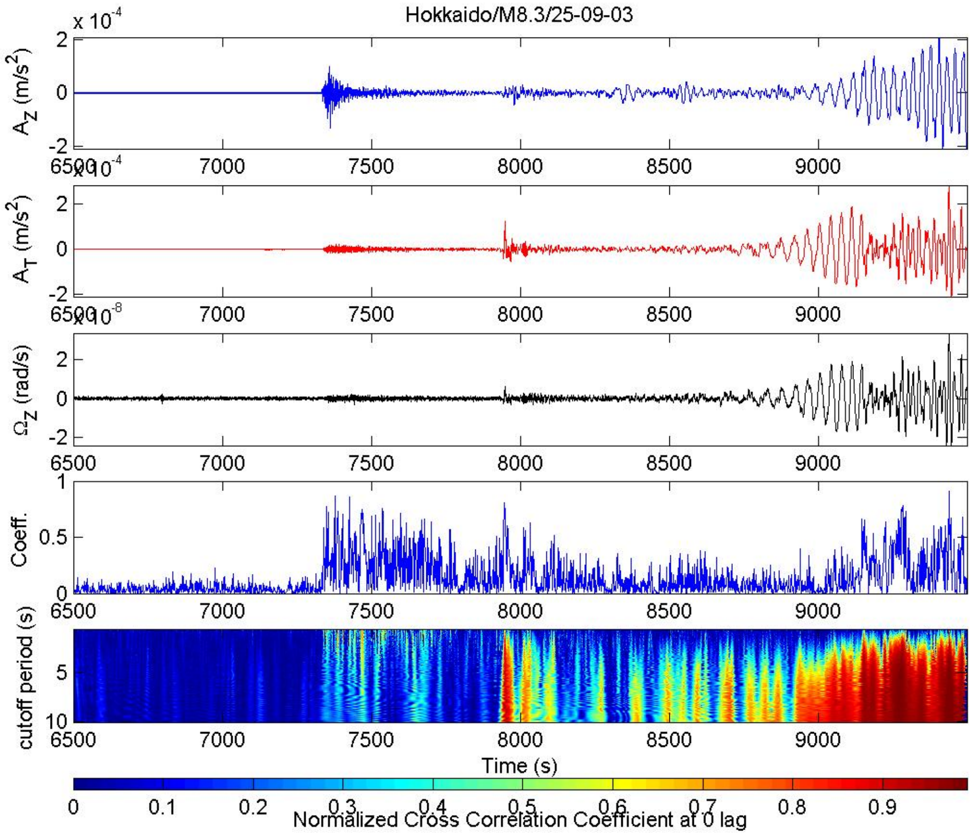

Figure 5. Hokkaido event 25/9/2003, M8.3. Top three traces: Vertical acceleration, transverse acceleration and rotation rate, respectively. The fourth trace (from top): zero lag normalized cross correlation coefficients calculated for time windows of 2s sliding along time series between rotation rate and transverse acceleration after high-pass filtering with cut-off period 1s. Bottom: the correlation coefficients as a function of time and cut-off period (length of sliding time window twice as long as the high pass cut off period applied before correlating).

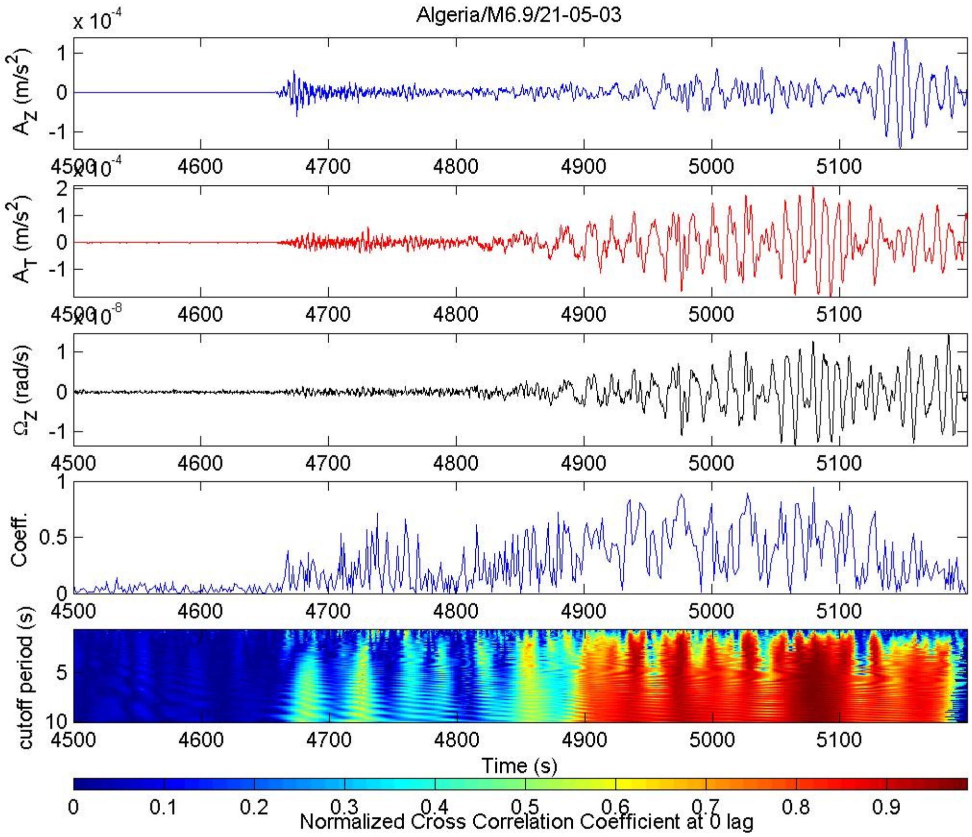

Figure 6. Algeria event 21/5/2003, M6.9. Top three traces: Vertical acceleration, transverse acceleration and rotation rate, respectively. The fourth trace (from top): zero lag normalized cross correlation coefficients calculated for time windows of 2s sliding along time series between rotation rate and transverse acceleration after high-pass filtering with cut-off period 1s. Bottom: the correlation coefficients as a function of time and cut-off period (length of sliding time window twice as long as the high pass cut off period applied before correlating).

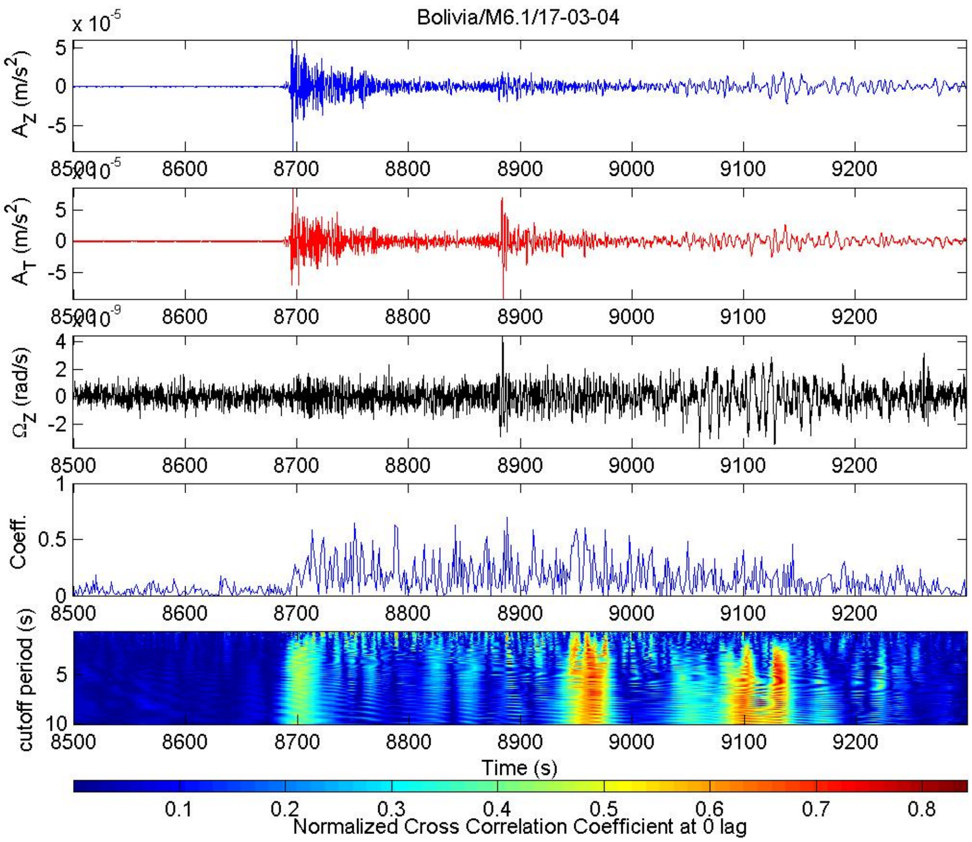

Figure 7. Bolivia event 17/3/2004, M6.1. Top three traces: Vertical acceleration, transverse acceleration and rotation rate, respectively. The fourth trace (from top): zero lag normalized cross correlation coefficients calculated for time windows of 2s sliding along time series between rotation rate and transverse acceleration after high-pass filtering with cut-off period 1s. Bottom: the correlation coefficients as a function of time and cut-off period (length of sliding time window twice as long as the high pass cut off period applied before correlating).

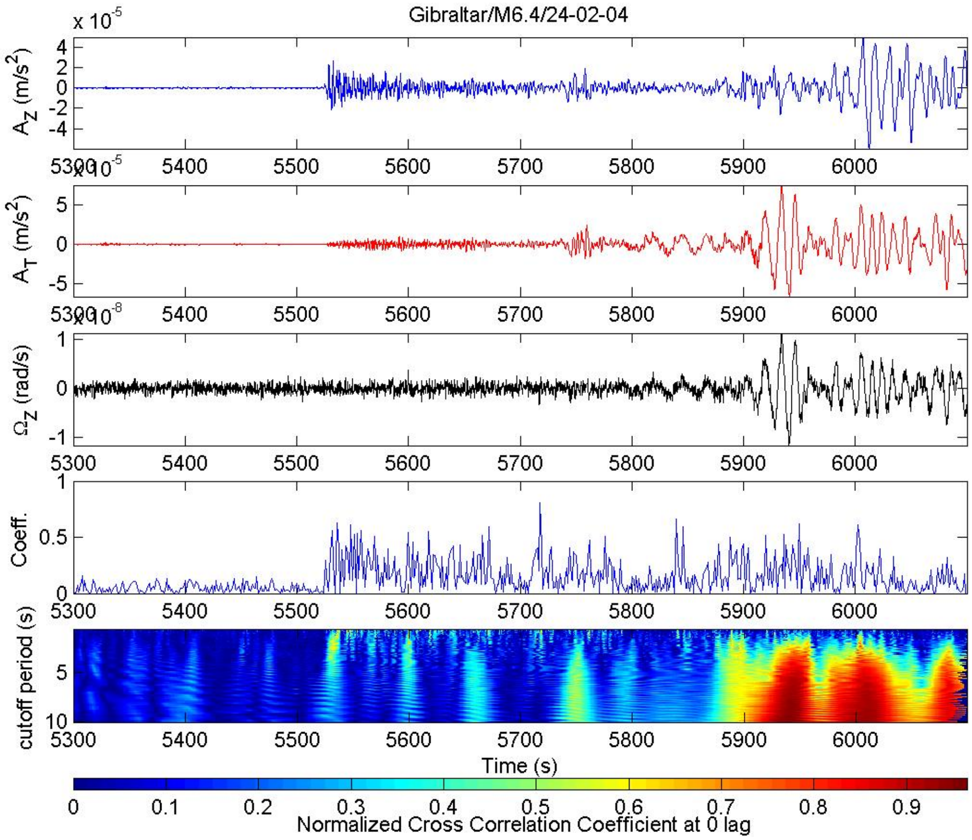

Figure 8. Gibraltar event 24/2/2004, M6.4. Top three traces: Vertical acceleration, transverse acceleration and rotation rate, respectively. The fourth trace (from top): zero lag normalized cross correlation coefficients calculated for time windows of 2s sliding along time series between rotation rate and transverse acceleration after high-pass filtering with cut-off period 1s. Bottom: the correlation coefficients as a function of time and cut-off period (length of sliding time window twice as long as the high pass cut off period applied before correlating).

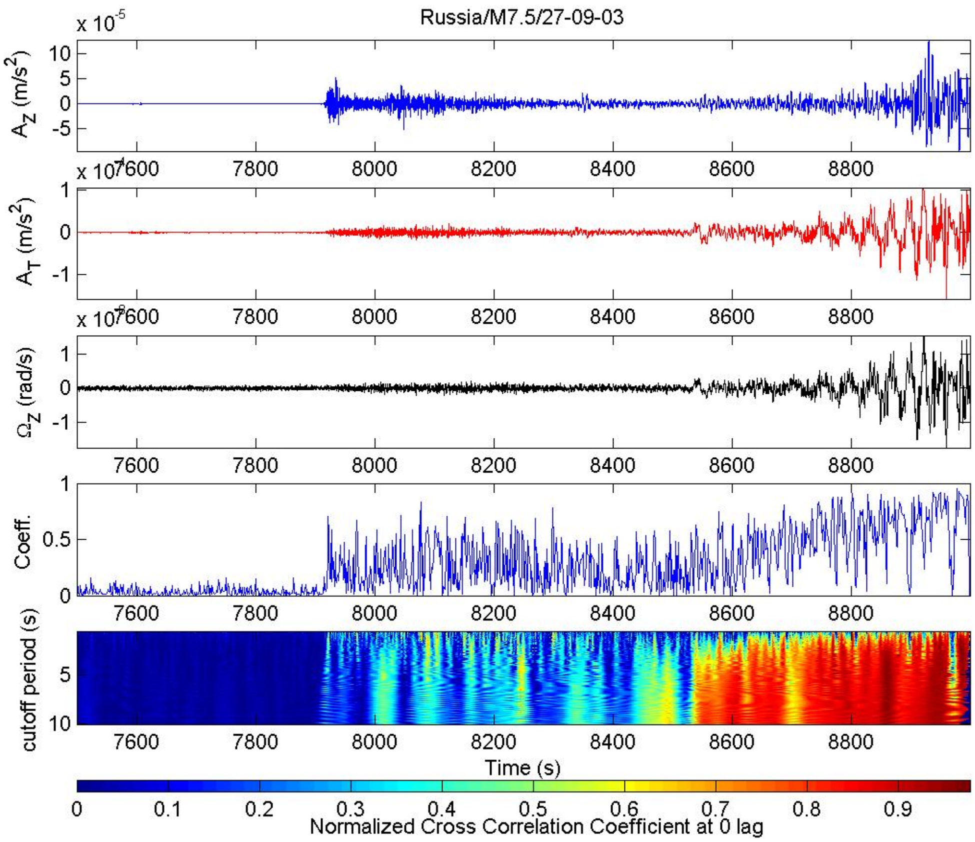

Figure 9. Russia event 27/9/2003, M7.5. Top three traces: Vertical acceleration, transverse acceleration and rotation rate, respectively. The fourth trace (from top): zero lag normalized cross correlation coefficients calculated for time windows of 2s sliding along time series between rotation rate and transverse acceleration after high-pass filtering with cut-off period 1s. Bottom: the correlation coefficients as a function of time and cut-off period (length of sliding time window twice as long as the high pass cut off period applied before correlating).

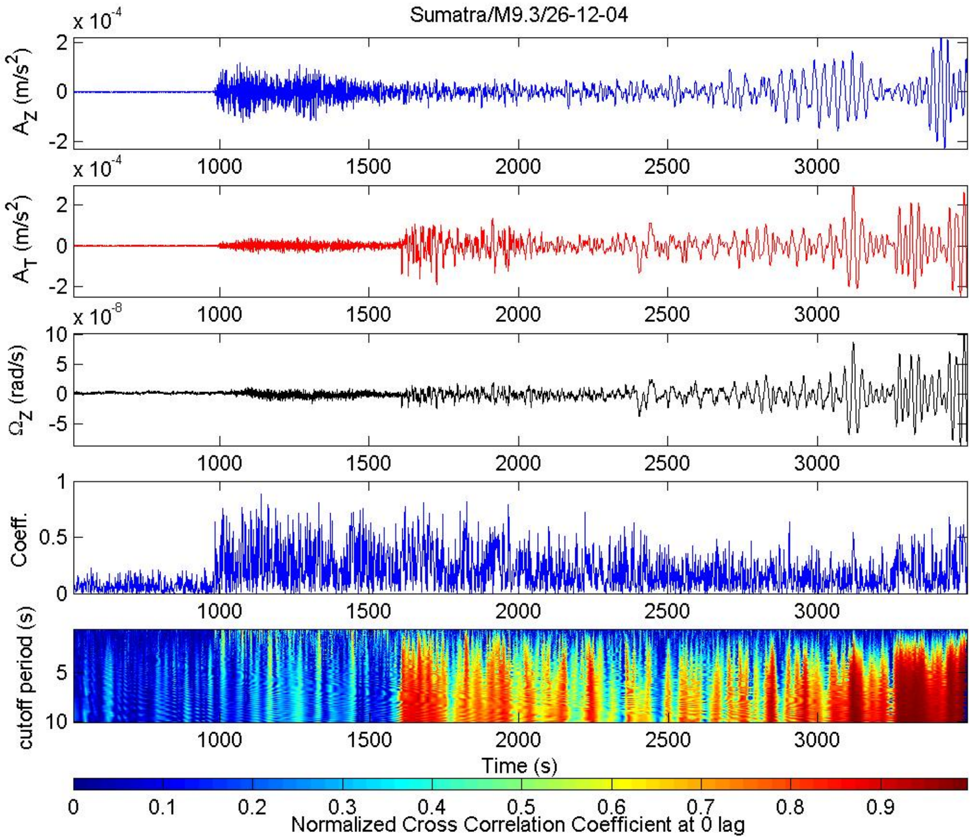

Figure 10. Sumatra event 26/12/2004, M9.3. Top three traces: Vertical acceleration, transverse acceleration and rotation rate, respectively. The fourth trace (from top): zero lag normalized cross correlation coefficients calculated for time windows of 2s sliding along time series between rotation rate and transverse acceleration after high-pass filtering with cut-off period 1s. Bottom: the correlation coefficients as a function of time and cut-off period (length of sliding time window twice as long as the high pass cut off period applied before correlating).

Table 1. Peak amplitudes of rotation and translation in the P coda from observed events

Event	Peak of A_Z in P coda [m/s^2] (pA_Z)	Peak of A_T in P coda [m/s^2] (pA_T)	Peak of Ω_Z in P coda [rad/s] ($p\Omega_Z$)	Ratio $pA_T/p\Omega_Z$	Ratio pA_T/pA_Z	Note for Ω_Z in P coda (N: noise; S: signal)
Afghanistan/M6.6/05-04-04	-2.13333E-06	9.48582E-07	7.60994E-10	1.247E+03	4.446E-01	N
Algeria/M6.9/21-05-03	-6.13000E-05	3.60621E-05	1.51629E-09	2.378E+04	5.883E-01	S
Bolivia/M6.1/17-03-04	-8.26667E-05	8.64104E-05	1.69708E-09	5.092E+04	1.045E+00	S (not very clear)
Gibraltar/M6.4/24-02-04	2.66333E-05	-7.56850E-06	2.15643E-09	3.510E+03	2.842E-01	N
Greece/M6.3/14-08-03	2.62667E-05	-1.35106E-05	1.20061E-09	8.907E+03	5.144E-01	S (not very clear)
Hokkaido/M8.3/25-09-03	-1.29433E-04	2.08227E-05	2.19760E-09	6.381E+03	1.609E-01	S
Honshu/M7.0/26-05-03	7.82000E-05	-1.10711E-05	7.43169E-10	1.368E+04	1.416E-01	S
Honshu/M7.0/31-10-03	8.96667E-06	-2.88125E-06	3.45293E-09	6.616E+02	3.213E-01	N
Honshu/M6.6/29-05-04	3.73333E-06	-1.14909E-06	5.67841E-10	1.901E+03	3.078E-01	N
Iran/M6.8/26-12-03	-7.66667E-06	2.88806E-06	7.68309E-09	3.759E+02	3.767E-01	N
Iran/M6.4/28-05-04	-2.42000E-05	-6.20838E-06	2.10504E-09	2.936E+03	2.565E-01	N
Irian-Jaya/M7.1/05-02-04	-2.46667E-06	2.43995E-06	4.69548E-10	5.196E+03	9.892E-01	N
Irian-Jaya/M7.5/07-02-04	2.40489E-06	-6.63333E-06	2.41502E-09	9.958E+02	3.625E-01	N
Ratislands/M7.8/17-11-03	2.41000E-05	-9.03502E-06	3.35164E-09	2.696E+03	3.749E-01	N
Russia/M7.5/27-09-03	5.15667E-05	1.03817E-05	1.29697E-09	8.005E+03	2.013E-01	S
Russia/M6.6/27-09-03	-1.49000E-05	3.84337E-06	1.01839E-09	3.340E+03	2.579E-01	N
Siberia/M7.1/01-10-03	-2.57000E-05	-6.23812E-06	1.02991E-09	4.637E+03	2.427E-01	N
Turkey/M5.7/06-07-03	-2.60000E-06	1.34024E-06	1.21156E-09	1.106E+03	5.155E-01	N
Germany/M5.0/05-12-04	1.14341E-04	-6.84344E-05	1.97923E-09	8.024E+03	5.985E-01	S
Sumatra/M9.3/26-12-04	-1.22598E-04	3.10074E-05	6.98199E-09	4.441E+03	2.529E-01	S